Materials Advances

ROYAL SOCIETY OF CHEMISTRY

PAPER

View Article Online
View Journal | View Issue

Check for updates

Cite this: *Mater. Adv.*, 2025, 6, 5286

# Predictive screening of phase stability in high-entropy ceramics†

Muhammad Waqas Qureshi, *[a] Shuguang Wei,[a] Longfei Liu,[a] Sudipta Paul,[a] Jun Young Kim,[a] Chuan Zhang,[b] Xudong Wang,[a] John H. Perepezko,[a] Dane Morgan[a] and Izabela Szlufarska*[a]

High-entropy materials offer unprecedented opportunities for tailoring mechanical, chemical, and thermal properties for enhanced performance across a multitude of applications, including energy storage, catalysis, and nuclear reactors. However, a major challenge in advancing their discovery lies in accurately predicting their single-phase stability and formation ability. Theoretically, phase stability can be predicted from free energies. In practice, this approach has been often unreliable for high-entropy materials because of limitations in the available experimental data needed to fit free energy terms. *Ab initio* calculations have been used to predict phase stability, but mostly by identifying descriptors that may correlate with stability. Here, we demonstrate that the phase stability of high-entropy ceramics can be accurately predicted by directly calculating free energy terms using *ab initio* calculations. The proposed approach is computationally efficient and physics-based and agrees with currently available experimental data. In the case of a composition where predictions of our models appeared inconsistent with the literature, we synthesized the sample experimentally and confirmed the accuracy of our models. We have also identified several new single-phase compositions of high-entropy ceramics that have not been previously reported. Our approach provides a new pathway for accelerating the design of high-entropy ceramics without the need for descriptors.

Received 30th January 2025,
Accepted 18th May 2025

DOI: 10.1039/d5ma00079c

rsc.li/materials-advances

Open Access Article. Published on 20 May 2025. Downloaded on 1/17/2026 11:19:57 PM.
This article is licensed under a Creative Commons Attribution 3.0 Unported Licence.

## 1. Introduction

High entropy materials (HEMs), also known as compositionally complex alloys, refer to alloys that have at least 5 principal elements with no dominant element that controls the properties. HEMs can be stabilized thermodynamically or kinetically in a single phase that is compositionally disordered.[1,2] In recent years, the family of HEMs has been rapidly expanding to include members that range from metallic alloys to ceramics, such as high-entropy alloys (HEAs),[3] carbides (HECs),[4] diborides (HEBs),[5–9] monoborides,[10] hexaborides,[11] oxides,[12,13] nitrides,[14,15] carbonitrides,[16] borocarbides,[17] and borocarbonitrides.[18] The occurrence of a single phase has been argued to arise from the substantial influence of configurational entropy,[1] although some recent reports have questioned this entropy stabilization explanation.[19–21] Nevertheless, for simplicity, we will continue referring to these materials as HEMs. Regardless of the underlying reason for stability, many HEMs have been successfully synthesized as the single phase and they have been shown to have many exceptional properties, including high thermal stability,[22] high strength coupled with ductility,[23,24] enhanced hardness,[25,26] and resistance to oxidation,[27] wear, and irradiation.[28,29] These properties arise from a combination of factors, including lattice distortion due to the atomic size mismatch, sluggish diffusion, and the stabilizing effect of high configurational entropy. The remarkable attributes of HEMs make them promising candidates for use in extreme environments, such as aerospace propulsion systems and nuclear fusion reactors, lightweight armors, high-performance cutting tools, thermal protection coatings, and a number of others.[30,31] Among the high-entropy ceramics, quinary HECs[32–41] have been studied most frequently, whereas quinary HEBs, exhibiting many similar properties, have rarely been studied. The first HEB with an $AlB_2$ structure was synthesized by Gild *et al.*[7] Since then, only a few other quinary HEB compositions with transition metals and rare-earth metals have been synthesized.[7–9,32,42–45]

A vast compositional space of high-entropy ceramics remains untapped due to lack of accurate and effective strategies for predicting their single-phase stability. For instance, experimental approaches are both time-consuming and costly, often relying heavily on physical intuition and expensive trial-and-error strategies. The thermodynamics for predicting phase

[a] *Department of Materials Science and Engineering, University of Wisconsin, Madison, WI, 53706, USA. E-mail: mwqureshi2@wisc.edu, szlufarska@wisc.edu*
[b] *CompuTherm LLC, Madison, WI, 53562, USA*

† Electronic supplementary information (ESI) available. See DOI: https://doi.org/10.1039/d5ma00079c



© 2025 The Author(s). Published by the Royal Society of Chemistry

Open Access Article. Published on 20 May 2025. Downloaded on 1/17/2026 11:19:57 PM. This article is licensed under a Creative Commons Attribution 3.0 Unported Licence.

stability is straightforward as the most stable phase is the one that has the lowest free energy. The challenge, however, lies in the ability to accurately determine the free energy expression. If sufficient experimental data are available, free energy terms can be fitted to such data as is done in CALPHAD-based methods. Indeed, the CALPHAD approach has been successfully applied in discovery of a number of HEMs.[46–48] However, CALPHAD is only accurate if data for developing the underlying databases are available, which can be a challenge for new alloys with five or more components.[49] An attractive alternative is to predict phase stability from *ab initio* calculations, but *ab initio* approaches have been used primarily to determine descriptors, which are quantities that are potentially correlated with phase stability. These *ab initio*-based descriptors include entropy forming ability (EFA),[4] disordered enthalpy–entropy descriptor (DEED),[32] and lattice distortion ($\delta$).[17] Other descriptors used in the literature but not based on *ab initio* energies are the valence electron concentration (VEC),[50] Zunger pseudopotential radii ($P_{rad}$),[51] and Pauling electronegativity difference ($\Delta\chi_{Pauling}$).[51] Some machine learning models[34,51] have also been trained using the latter list of descriptors. The most promising of these descriptors based on the literature[32] are EFA and DEED. EFA has been developed to predict HECs[4] and it is meant to capture a correlation between the width of the enthalpy distribution of sampled configurations and phase stability, where a narrow energy distribution corresponds to a single phase. The DEED is an extension of EFA and it has been applied to predict single-phase stability in HEBs and HECNs.[32] The threshold values of EFA and the DEED were determined self-consistently from available experiments. While descriptor-based approaches showed consistency with available experiments across different ceramic categories and the descriptors are physically motivated, descriptors make the significant use of empirical correlations instead of primarily physics-based modeling. This can lead to inaccuracies and leaves no clear pathway to improvement when new compositions are synthesized, and discrepancies are uncovered in predicting phase stability.

Here, we propose a free energy model based on *ab initio* calculations for predicting the phase stability of quinary high-entropy ceramics (HEBs and HECs). The thermodynamic stability of the multicomponent system is evaluated based on Gibb's free energies of the disordered high-entropy phase relative to those of competing phases. Our model is based on fundamental thermodynamic principles, provides accurate and computationally efficient predictions compared to available descriptors, and can easily be improved with more detail free energy modeling. The model is validated on existing data, used to guide new experiments to correct some previous experiments, and then used to predict several new HEB candidates that can form the single phase.

## 2. Materials and methods

### 2.1. *Ab initio*-based free energy model

In the free energy expression, $\Delta G = \Delta H - T\Delta S$, $\Delta H$ is the enthalpy change associated with forming the high-entropy material. Here, we calculated enthalpy with respect to most stable competing phases by considering all the potential decomposition products within the Materials Project[52] database, including elemental, binary, ternary and so on:

$$\Delta H = H_{\text{compound}} - H_{\text{cHull}}$$

where $H_{\text{compound}}$ is the enthalpy of a target high-entropy disordered system and $H_{\text{cHull}}$ is the convex hull energy at that composition, respectively. The entropy is calculated assuming the ideal mixing approximation:

$$\Delta S = -R \sum c_i \ln c_i$$

where $R$ is the gas constant and $c_i$ is the molar fraction of the $i$th element. $\Delta S$ is normalized by the stoichiometry of diboride (or binary carbide) in the free-energy model, because the anion sublattice remains unchanged and does not contribute to the total configurational entropy. In our calculations, entropy terms for the decomposition products are not considered. The convex hull analysis is performed using the pymatgen library,[53] ensuring the rigorous evaluation of the thermodynamic landscape of the high-entropy system.

### 2.2. First-principles calculations

All first-principles calculations were performed within the framework of DFT, implemented using the Vienna ab initio simulation package (VASP).[54] The projected-augmented-wave with the Perdew–Burke–Ernzerhof (PBE) form of exchange–correlation potentials was used to treat the electronic interactions with ions and the electron exchange–correlation functionals.[55,56] To create random structures, the special quasirandom structure (SQS)[57] approach was adopted, with the SQS found using the Monte Carlo method (mcsqs) available through the alloy theoretic automated toolkit (ATAT).[58] A supercell of $5 \times 5 \times 3$ and $3 \times 3 \times 3$ was used for borides and carbides, respectively, in which all metal lattice sites were occupied by 5 different elements that form equimolar quinary HEMs (Fig. 1b and d). For the optimization of SQS structures, the conjugate gradient method is used keeping the calculation parameters consistent with the materials project[59] with a plane-wave cut-off energy of 520 eV. The Broyden Fletcher–Goldfarb–Shanno (BFGS)[60] algorithm was used to obtain the ground state atomic configuration with an energy tolerance of 0.002 meV atom$^{-1}$.

Equilibrium phase diagrams of quinary HEBs and HECs were calculated using the recently updated PanRHEA2023b thermodynamic database and Pandat software (version 2023)[61] developed by CompuTherm, LLC. The PanRHEA2023b database contains 22 elements with 509 phases and has complete thermodynamic descriptors for all the binary systems (especially metal diborides and carbides) which build up the quinary high-entropy ceramic systems explored in this work.

### 2.3. Sample preparation and characterization

Four binary carbide powders (TiC, ZrC, HfC, and $Mo_2C$), W powders and graphite powders with a purity of more than 99% were used as precursors for the synthesis of the (TiZrHfMoW)C

Open Access Article. Published on 20 May 2025. Downloaded on 1/17/2026 11:19:57 PM.
This article is licensed under a Creative Commons Attribution 3.0 Unported Licence.

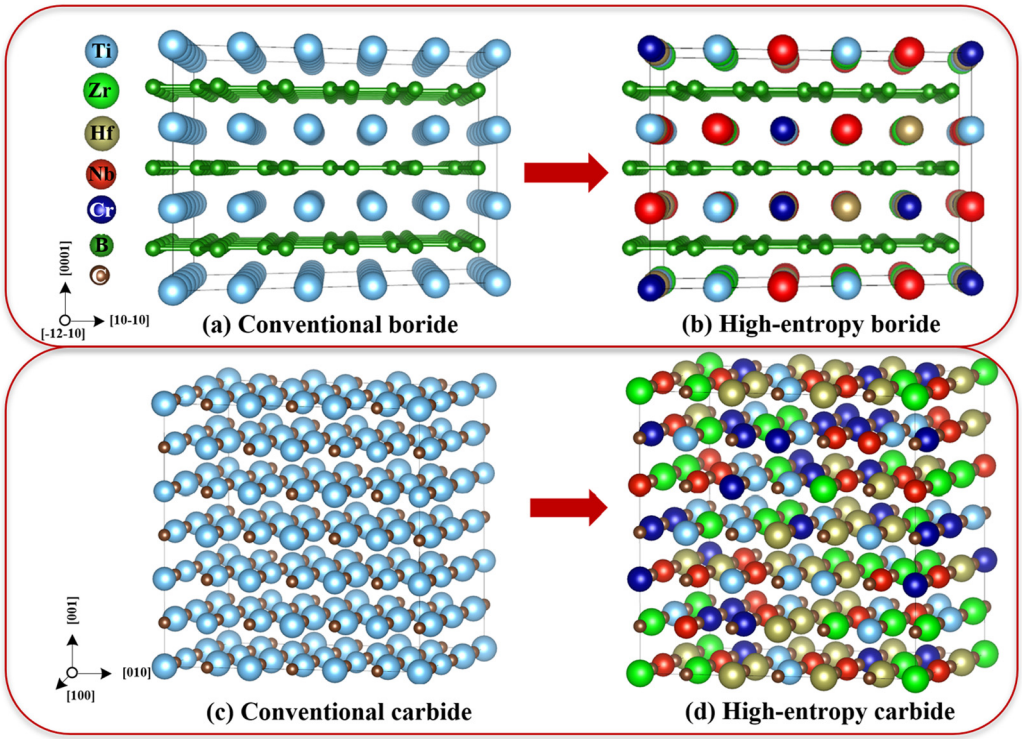


Fig. 1 Schematic illustration of the atomic structure. (a) Conventional diboride, (b) high-entropy boride, (c) conventional carbide, and (d) high-entropy carbide. (b) and (d) The metal cations are randomly occupied by Ti (sky blue), Zr (light green), Hf (gold), Nb (red), and Cr (blue).

sample. The precursors were weight measured in a stoichiometric amount and powder mixtures were then subjected to high-energy ball milling using $Si_3N_4$ milling media in $Si_3N_4$ jars. Milling was conducted in an ethanol medium and in a sequence of 5 minutes of milling and 5 minutes of rest to avoid overheating to a total of 2 hours. The mixed powders were dried at 65 °C and then arc-melted in argon and cooled on a water-cooled copper hearth. The bulk sample was cut using a wafering blade and a mirror polished on one side using diamond lapping film discs. To homogenize the samples, we performed thermal annealing on the arc-melted samples for 12 hours in a vacuum ($10^{-5}$ Pa) at 1650 °C. The sample was furnace-cooled with a cooling rate of 300 °C minute$^{-1}$.

To confirm that the arc-melted sample is in the single phase, we carried out XRD analysis on the polished surface of the sample using a Bruker D8 discovery X-ray diffractometer equipped with a two-dimensional detector. For the XRD test, the scan range ($2\theta$) was set to be 20°–80° with a step of 20° and at least 120 s for each step. In addition, scanning electron microscopy (SEM) based energy dispersive spectroscopy (EDS) was performed on the arc-melted (TiZrHfMoW)C sample using an FEI Helios PFIB G4 equipped with an Thermo Noran energy dispersive X-ray microanalysis system operated at 10 kV.

## 3. Results

### 3.1. Free-energy model

The thermodynamic stability of a system is fundamentally governed by its Gibb's free energy, $\Delta G = \Delta H - T\Delta S$, where $\Delta H$, $T$, and $\Delta S$ are the enthalpy, the absolute temperature, and the entropy, respectively. We determine $\Delta H$ of the disordered phase relative to the most stable decomposition products, by carrying out DFT calculations of the energy above the convex hull (cHull). In these calculations, we considered random arrangements of the metal atoms in the HEBs and HECs and all possible competing phases encompassing elemental, binary, and ternary compositions in the Materials Project database.[59] To enable rapid calculations, we chose a simple ideal solution approximation to the entropic contribution ($\Delta S$) for possible disordered sublattices of the HEBs and HECs, which is consistent with the random arrangements used in the enthalpy calculations. The model predicts the phase stability at the temperature ($T$) used in the calculation of the free energy, with $\Delta G < 0$ implying the single phase and $\Delta G > 0$ implying the multiphase. However, we will be comparing to whether a cooled sample at room temperature is in the single or multi-phase, which is the typical categorization of HEMs. The phase stability of such cooled samples is set by the last temperatures the materials experienced during which there were adequate kinetics for at least some equilibration. For the HEB and HEC experimental data discussed in this paper, all samples were synthesized in the range of 1800–2200 °C and then furnace cooled, thus taking some time (depending on the cooling rate) to reach to room temperature. We are therefore looking for the lowest temperature at which the system can have significant kinetics, $T_k$, to allow for phase separation. $T_k$ is not known in general but for sintering and annealing of ceramics it is typically taken as approximately half of the melting point,[62,63]


© 2025 The Author(s). Published by the Royal Society of Chemistry

Open Access Article. Published on 20 May 2025. Downloaded on 1/17/2026 11:19:57 PM. This article is licensed under a Creative Commons Attribution 3.0 Unported Licence.

which corresponds to the range of 1200–1600 °C. In this work, we estimate $T_k$ using the very general principle that diffusion kinetics is strongly correlated with melting temperature. Specifically, for a given composition, we assume that $T_k$ is a linear function of the average melting point of individual binary carbides and diborides and set the slope and intercept so that $T_k$ is in the range of 1200–1600 °C. The binary melting points used, their averages and the values of $T_k$ for all the materials discussed in this paper, and the functions giving $T_k$ along with the sensitivity analysis of our model with respect to $T_k$ are given in Table S1 and Section SI (ESI†). This is obviously an approximate model and further work modeling the kinetics of these alloys might provide a significant improvement. Together these approximations are consistent with assuming that short-range-order and vibrational (including zero-point energy) and electronic excitations do not play a critical role in the stability calculations, either due to being small contributions or undergoing significant cancellation, and that the results are not sensitive to the exact temperature range where kinetics cease. These are significant approximations, and we at least partially account for their influence by defining a ''buffer'' region of 20 meV atom$^{-1}$ around $\Delta G = 0$ for which we do not consider the predictions of the single or multiphase to be reliable.

### 3.2. Strategy for selecting compositions

In this study, we are focusing on HEBs and HECs. The conventional metal diboride exhibits a layered hexagonal crystal structure ($AlB_2$-type, space group: *P*6/*mmc*, #191) with an alternating two-dimensional (2D) boron network and a 2D layer occupied by a transition metal (Fig. 1a). HEBs maintain the same crystal structure, but now the metal sublattice is occupied by elements that form a solid solution (Fig. 1b). Similarly, HECs adopt a structure of binary carbides (Fig. 1c) with a face centered cubic (FCC) rock-salt type structure (space group $Fm\bar{3}m$, #225), except that in HECs the metal sub-lattice forms a solid solution (Fig. 1d). Numerous HEC compositions have been synthesized experimentally[4,32–41,64] and we have selected those compositions for applying our free-energy based stability screening. In applying our free-energy based screening to HEBs, we also include all known HEB compositions that have been synthesized. However, since there have been relatively few HEB compositions synthesized experimentally,[7–9,32,42–44] we complement these compositions by including additional candidate materials. In expanding the compositional space, we constrained the selection to three fixed elements: Ti, Zr, and Hf. The remaining two elements are chosen from the early-(V, Nb, Ta, Cr, Mo, and Mn) and late-(Fe, Co, and Ni) transition metal elements along with one A-group element (Al). For convenience, we adopted the nomenclature HEB-$M_4M_5$, where $M_4$ and $M_5$ represent the selected elements outside of the Ti, Zr, and Hf, *e.g.*, HEB-NbCr represents the composition $(Ti_{0.2}Zr_{0.2}Hf_{0.2}Nb_{0.2}Cr_{0.2})B_2$. We focus on HEBs and HECs with 5 components; however, to demonstrate the applicability of our model, we have also included a few examples of quaternary systems that have been already synthesized experimentally.[65]

Selection of the HEB elements is motivated by several key factors. Refractory metals are included because their binary metal-diborides ($MB_2$) have excellent thermal stability (melting point at ~3000 °C), relatively high hardness (~16–28 GPa), and good oxidation resistance, and they are being considered for applications in corrosive[66,67] and radiation[68] related environments. Aluminum (Al) is selected due to its ductility and ability to form $Al_2O_3$, which could enhance both the fracture toughness and the oxidation resistance. Despite these potential advantages, Al-based HEBs have not yet been explored in the literature and therefore the current study can provide useful guidance for the synthesis of novel borides. The selection of Ni, Co, and Fe within our composition space is guided by previous findings which showed that a weaker M–B bond is beneficial to defect recovery processes in MB and MAB phases,[69] potentially improving their radiation tolerance[70,71] (M is the transition metal, A is Al, and B is boron). Following a similar approach to ref. 69, we have selected Ni, Co and Fe since these elements have relatively weak M–B bond separation energy (see Fig. S2, ESI†). This strategic selection of different elements enables tailoring and optimizing the HEB properties in response to high-temperature and radiation-intensive environment.

### 3.3. Free energy of high-entropy ceramics

We evaluated free energies using our approach for all the HEB and HEC compositions discussed above. Fig. 2a shows the estimated free energies of HEBs. The data are ordered by increasing $\Delta G$ and naturally divides the systems into two groups based on the positive and negative values of $\Delta G$, corresponding to predictions of multi- and single-phase compositions, respectively. The grey region near $\Delta G = 0$ represents regions where we consider the prediction to be uncertain within our accuracy (see discussion above). Compositions that have been synthesized experimentally are marked with a star. From the reported experimental data, we excluded W-based HEBs[5,7–9,32,44,72,73] because the experimental results are inconsistent with each other, with both single- and multi-phase HEBs reported for the same composition. More details are provided in Section III of the ESI.† Our model agrees well with the remaining experiments, except for (HfMnTiVZr)B2, which has been reported to be the multi-phase in earlier experiments[32] (indicated by the blue arrow in Fig. 2a). However, the experimental results could be uncertain because the $MnO_2$ precursor used in synthesis has a much lower melting temperature (535 °C) than the synthesis temperature (1900 °C). Under the synthesis conditions, $MnO_2$ becomes volatile and it is not entirely clear how much Mn remained in the samples since detailed chemical analysis of synthesized samples was not reported by the authors of ref. 32. A detailed summary of experimental findings and our predictions is given in Table S2 (ESI†).

We have also compared predictions of our model to phase stability determined from CALPHAD phase diagrams (Fig. 2b). Our free-energy predictions agree with CALPHAD except for two compositions marked by pink bars: HEB-FeTa and HEB-FeMo, where our model predicts a single-phase and CALPHAD

Open Access Article. Published on 20 May 2025. Downloaded on 1/17/2026 11:19:57 PM.
This article is licensed under a Creative Commons Attribution 3.0 Unported Licence.

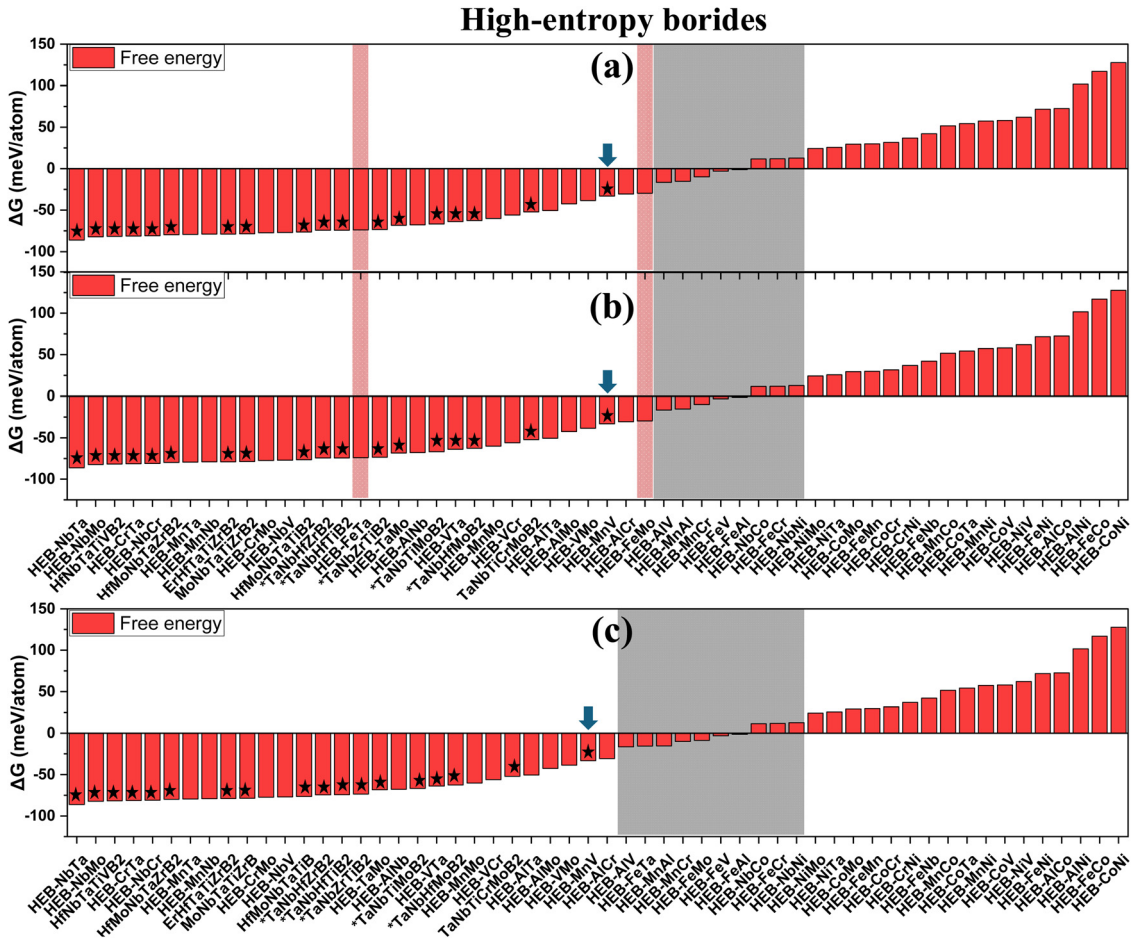


Fig. 2 Predictions of phase stability in HEBs. (a) Free energies of HEBs calculated using the *ab initio* based free energy model. Stars represent experimentally synthesized compositions. Arrows indicate a prediction from our model that seemingly disagrees with experiments. (b) The same data as in (a), with added comparison to CALPHAD (pink vertical bars). (c) The same data as in (b) but with mixing terms artificially removed from the *ab initio* based free energy model for compositions marked with pink bars in (b). Compositions in (c) are re-ordered relative to those in (b) to keep $\Delta G$ monotonic. (c) Predictions from the free energy model agree with CALPHAD phase diagrams. The composition labels are the same in (a) and (b). The compositions with * in their names are the quaternary compositions with 4-components. The grey region marks a 20 meV atom$^{-1}$ buffer where predictions of the model might be uncertain due to approximations in free energy calculations.

predicts a multi-phase HEB. Since both our approach and CALPHAD are based on a physical description of free energies, it is possible to compare details of the models when a discrepancy is observed. Toward this end, we found that CALPHAD is missing mixing enthalpies for binary interactions in each of the two compositions that show discrepancies with our model. When we artificially removed these mixing terms from our model the resulting predictions became consistent with those from CALPHAD (Fig. 2c). CALPHAD is typically optimized up to three-component systems and extrapolates the description of all subsystems to higher-order systems.[49] Thus, reliable thermodynamic descriptions of many component alloys are often incomplete or entirely missing, which leads to potentially large extrapolation errors. The limitations of the current CALPHAD database for high entropy systems are beyond the scope of this study and are well discussed in other papers.[74,75] It is therefore reasonable to conclude that the disagreement between our model and CALPHAD arises from the current limitations in the thermodynamic database in CALPHAD. Our analysis predicts a total of 21 HEBs that could potentially be stable in single-phase solid solutions (see Table S3, ESI†).

Predictions of phase stability for HECs using our *ab initio* based free energy model are shown in Fig. 3a. Stars indicate the HEC compositions reported in earlier experimental studies.[4,32–41] Our predictions are in agreement with experimental data, except for compositions indicated by arrows. These compositions are predicted to be single-phase in our model, while experimental reports classify them as multi-phase, or *vice versa*.[40] Interestingly, all these outliers contain W. Given the challenges associated with synthesizing W-based HEBs, as discussed above, it is reasonable to ask whether similar challenges exist for W-based HECs. To help answer this question, we have synthesized (TiZrHfMoW)C, which is a W-containing HEC that showed apparent disagreement between predictions of our model and experiments. Furthermore, this composition was our weakest prediction of stabilization of the


© 2025 The Author(s). Published by the Royal Society of Chemistry

Open Access Article. Published on 20 May 2025. Downloaded on 1/17/2026 11:19:57 PM.
This article is licensed under a Creative Commons Attribution 3.0 Unported Licence.

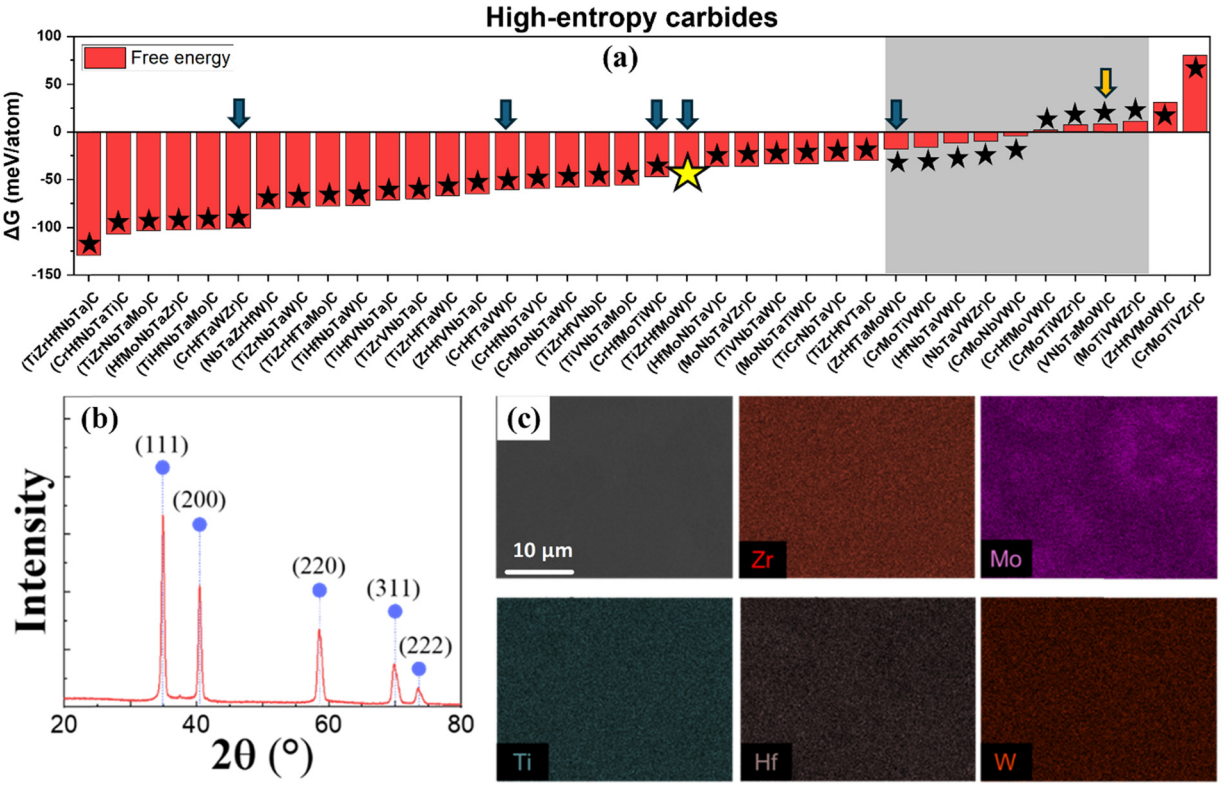


Fig. 3 Predictions of phase stability in HECs. (a) Free energies predicted using the *ab initio* based free energy model with negative and positive values of $\Delta G$ indicating single- and multi-phase stability, respectively. Black stars mark experimental data available in the literature. Arrows indicate compositions where published experimental data seemingly disagree with predictions of our model, all W-based HECs. Yellow star marks the HEC composition ((TiZrHfMoW)C) synthesized by us that confirms predictions of our model. The grey region marks a 20 meV buffer and represents uncertainty in the predictions of the model. (b) XRD spectra for (TiZrHfMoW)C showing a single-phase FCC system. (c) Microstructure of (TiZrHfMoW)C from SEM analysis and the elemental distribution of five cations from SEM-based EDS analysis.

four discrepancies outside the buffer zone, giving it the largest chance of being an erroneous prediction of our model. This composition is predicted to be the multiphase in experiments[7–9] and descriptor-based screening[32] (indicated with a yellow start in Fig. 3a).

The X-ray diffraction (XRD) spectrum for (TiZrHfMoW)C synthesized in the current study is shown in Fig. 3b and it exhibits peaks consistent with a single-phase FCC high-entropy phase. We have also imaged the microstructure of the synthesized sample using scanning electron microscopy (SEM) and found no second phase precipitates (Fig. 3c). In addition, the elemental distribution of the five cations was analyzed using SEM-based energy dispersive X-ray spectroscopy (EDS). The elemental map is shown in Fig. 3c, and it confirms that all metal elements are distributed uniformly in the sample. The EDS point scan was also carried out in (TiZrHfMoW)C to confirm the stoichiometry of elements (Fig. S3 and Table S4, ESI†). This observation of a single phase in experimentally synthesized (TiZrHfMoW)C confirms predictions of our *ab initio* based free energy model and underscores challenges associated with the experimental synthesis of W-based HEBs and HECs. Our predictions for HECs have also been compared to those based on CALPHAD calculations (see Fig. S4, ESI†) and similarly to what was shown for HEBs (Fig. 2b), predictions from the two models disagree for a few compositions. In many cases, CALPHAD is missing the mixing terms for interactions between binary phases of HEBs and HECs, as discussed earlier.

Our *ab initio* based free energy model provides a complimentary approach to DFT-based descriptors in predicting phase stability. Applicability of the most recent descriptors, EFA and DEED, to our data is shown in section VI of the ESI.† Our approach has a couple of advantages relative to the descriptors. One is that it is computationally less costly. For example, the descriptor-based approach requires the enthalpies of 49 and 82 unique configurations to obtain the energy distribution (needed for EFA and the DEED) for each composition of HECs and HEBs, respectively. In contrast, our model requires the enthalpy of a single randomized supercell of a target composition. Secondly, if needed, our model has a clear path for further improvement and development. As more high-entropy ceramics are synthesized, it is in fact expected that our model may show some discrepancies with experimental data, especially near $\Delta G = 0$. These discrepancies could arise from our ideal solution approximations and come from short-range ordering and vibrational and electronic excitations. One of the possible reasons for the discrepancies may be that the synthesized sample did not reach the state of fully equilibrium. Qualitatively, we predict stability under approximate synthesis

Open Access Article. Published on 20 May 2025. Downloaded on 1/17/2026 11:19:57 PM. This article is licensed under a Creative Commons Attribution 3.0 Unported Licence.

conditions by considering the temperature $T_k$ at which kinetics freezes out during experimental cooling. If the equilibrium phase is reached during experimental synthesis, the predictions of the model are expected to be consistent with experiments. Our general approach was to exclude experimental data with conflicting results from comparison to our model. In selected cases where we suspected that the equilibrium might not have been reached in reported experiments, we carried out our own experiments with a longer annealing time and were able to confirm predictions of our model. Discrepancies could also come from our approximate treatment of the temperature for kinetics freezing in the material or just DFT errors. To avoid overinterpreting predictions from $\Delta G$ near 0, we have introduced a buffer region that flags any prediction less than 20 meV atom$^{-1}$ as not robust. To support this 20 meV atom$^{-1}$ range, we note that it is consistent with the effect of short-range ordering from more detailed calculations. Specifically, in ref. 76, we have carried out hybrid molecular dynamic Monte-Carlo (MD/MC) simulations with a machine learning potential to confirm the existence of short-range ordering in (NbTiVZr)C and (NbTiVMo)C[76]. We found that the change in the potential energies from the random solid solutions to short-range ordering is approximately 15 meV atom$^{-1}$ and 13 meV atom$^{-1}$ for (NbTiVZr)C and (NbTiVMo)C, respectively, which is within the limit of the 20 meV atom$^{-1}$ buffer zone we included here in the free-energy model. Further improvements of the model can include calculating vibrational $^{77}$d electronic contributions to the entropy, accounting for free energy changes associated with the likely presence of chemical short-range ordering,[76,77] and more realistic modeling of the kinetics during cooling.

## 4. Conclusions

We have developed an approach to determine the phase stability of high-entropy ceramics using an *ab initio* based free-energy model. The model was approximate and used the zero-temperature enthalpic contributions of the most stable competing phases and an ideal mixing approximation for the entropy, but we have shown that it is accurate enough that our predictions are in a very good agreement with available experimental data. We have then used the model to predict several new single-phase high-entropy compositions. We confirmed our free-energy prediction by successfully synthesizing single-phase (TiZrHfMoW)C which was previously reported as multi-phase in experiments as well as descriptor-based studies. In conclusion, our study provides a physic-based model that can be evaluated efficiently with modest computational resources using *ab initio* simulations. This approach has been validated for HEBs and HECs, and the next step will be to explore its applicability to other classes of high-entropy materials.

## Data availability

The data that support the findings of this study are available from the corresponding author upon reasonable request.

## Conflicts of interest

There are no conflicts to declare.

## Acknowledgements

This work is supported by the Department of Energy Basic Energy Science Program (Grant No. DEFG02-08ER46493). This work used the TACC's Stampede3 at the University of Texas at Austin through allocation TG-MAT240078, from the Advanced Cyberinfrastructure Coordination Ecosystem: the Services & Support (ACCESS)[78] program, which is supported by the National Science Foundation (NSF) grants #2138259, #2138286, #2138307, #2137603, and #2138296. Support for D. M. was provided by the National Science Foundation under the Award Number 1931298, titled ''Collaborative Research: Framework: Machine Learning Materials Innovation Infrastructure''.

## References

1 J. W. Yeh, S. K. Chen, S. J. Lin, J. Y. Gan, T. S. Chin, T. T. Shun, C. H. Tsau and S. Y. Chang, *Adv. Eng. Mater.*, 2004, **6**, 299–303.
2 B. Cantor, I. T. H. Chang, P. Knight and A. J. B. Vincent, *Mater. Sci. Eng., A*, 2004, **375–377**, 213–218.
3 M. H. Tsai and J. W. Yeh, *Mater. Res. Lett.*, 2014, **2**, 107–123.
4 P. Sarker, T. Harrington, C. Toher, C. Oses, M. Samiee, J. P. Maria, D. W. Brenner, K. S. Vecchio and S. Curtarolo, *Nat. Commun.*, 2018, **9**, 1–10.
5 L. Feng, F. Monteverde, W. G. Fahrenholtz and G. E. Hilmas, *Scr. Mater.*, 2021, **199**, 113855.
6 Y. Zhang, S. K. Sun, W. M. Guo, W. Zhang, L. Xu, J. H. Yuan, D. K. Guan, D. W. Wang, Y. You and H. T. Lin, *J. Eur. Ceram. Soc.*, 2021, **41**, 1015–1019.
7 J. Gild, Y. Zhang, T. Harrington, S. Jiang, T. Hu, M. C. Quinn, W. M. Mellor, N. Zhou, K. Vecchio and J. Luo, *Sci. Rep.*, 2016, **6**, 2–11.
8 J. Gild, A. Wright, K. Quiambao-Tomko, M. Qin, J. A. Tomko, M. Shafkat bin Hoque, J. L. Braun, B. Bloomfield, D. Martinez, T. Harrington, K. Vecchio, P. E. Hopkins and J. Luo, *Ceram. Int.*, 2020, **46**, 6906–6913.
9 Y. Zhang, S. K. Sun, W. Zhang, Y. You, W. M. Guo, Z. W. Chen, J. H. Yuan and H. T. Lin, *Ceram. Int.*, 2020, **46**, 14299–14303.
10 M. Qin, Q. Yan, H. Wang, C. Hu, K. S. Vecchio and J. Luo, *Scr. Mater.*, 2020, **189**, 101–105.
11 M. Qin, Q. Yan, Y. Liu, H. Wang, C. Wang, T. Lei, K. S. Vecchio, H. L. Xin, T. J. Rupert and J. Luo, *J. Eur. Ceram. Soc.*, 2021, **41**, 5775–5781.
12 C. H. Tsau, Y. C. Yang, C. C. Lee, L. Y. Wu and H. J. Huang, *Procedia Eng.*, 2012, **36**, 246–252.
13 C. M. Rost, E. Sachet, T. Borman, A. Moballegh, E. C. Dickey, D. Hou, J. L. Jones, S. Curtarolo and J.-P. Maria, *Nat. Commun.*, 2015, **6**, 8485.
14 T. Jin, X. Sang, R. R. Unocic, R. T. Kinch, X. Liu, J. Hu, H. Liu, S. Dai, T. Jin, X. F. Liu, J. Hu, H. L. Liu, S. Dai,

 © 2025 The Author(s). Published by the Royal Society of Chemistry

Open Access Article. Published on 20 May 2025. Downloaded on 1/17/2026 11:19:57 PM. This article is licensed under a Creative Commons Attribution 3.0 Unported Licence.

X. H. Sang, R. R. Unocic and R. T. Kinch, *Adv. Mater.*, 2018, **30**, 1707512.
15 T. K. Chen, T. T. Shun, J. W. Yeh and M. S. Wong, *Surf. Coat. Technol.*, 2004, **188–189**, 193–200.
16 Y. Wang, T. Csanádi, H. Zhang, J. Dusza and M. J. Reece, *Acta Mater.*, 2022, **231**, 117887.
17 D. Hedman, A. C. Feltrin, Y. Miyamoto and F. Akhtar, *J. Mater. Sci.*, 2022, **57**, 422–443.
18 J. Guan, D. Li, Z. Yang, B. Wang, D. Cai, X. Duan, P. He, D. Jia and Y. Zhou, *Ceram. Int.*, 2020, **46**, 26581–26589.
19 S. S. Aamlid, M. Oudah, J. Rottler and A. M. Hallas, *J. Am. Chem. Soc.*, 2023, **145**, 5991–6006.
20 A. Sarkar, B. Breitung and H. Hahn, *Scr. Mater.*, 2020, **187**, 43–48.
21 D. B. Miracle and O. N. Senkov, *Acta Mater.*, 2017, **122**, 448–511.
22 F. Wang, X. Zhang, X. Yan, Y. Lu, M. Nastasi, Y. Chen and B. Cui, *J. Am. Ceram. Soc.*, 2020, **103**, 4463–4472.
23 S. Chen, Z. H. Aitken, S. Pattamatta, Z. Wu, Z. G. Yu, D. J. Srolovitz, P. K. Liaw and Y. W. Zhang, *Nat. Commun.*, 2021, **12**, 1–11.
24 Y. F. Ye, Q. Wang, J. Lu, C. T. Liu and Y. Yang, *Mater. Today*, 2016, **19**, 349–362.
25 M. Qin, S. Shivakumar, T. Lei, J. Gild, E. C. Hessong, H. Wang, K. S. Vecchio, T. J. Rupert and J. Luo, *J. Eur. Ceram. Soc.*, 2022, **42**, 5164–5171.
26 Y. Wang, T. Csanádi, H. Zhang, J. Dusza, M. J. Reece and R. Z. Zhang, *Adv. Theory Simul.*, 2020, **3**, 2000111.
27 H. Wang, X. Han, W. Liu and Y. Wang, *Ceram. Int.*, 2021, **47**, 10848–10854.
28 F. Wang, X. Yan, T. Wang, Y. Wu, L. Shao, M. Nastasi, Y. Lu and B. Cui, *Acta Mater.*, 2020, **195**, 739–749.
29 Z. Cheng, J. Sun, X. Gao, Y. Wang, J. Cui, T. Wang and H. Chang, *J. Alloys Compd.*, 2023, **930**, 166768.
30 C. Oses, C. Toher and S. Curtarolo, *Nat. Rev. Mater.*, 2020, **5**, 295–309.
31 E. J. Pickering, A. W. Carruthers, P. J. Barron, S. C. Middleburgh, D. E. J. Armstrong and A. S. Gandy, *Entropy*, 2021, **23**, 98.
32 S. Divilov, H. Eckert, D. Hicks, C. Oses, C. Toher, R. Friedrich, M. Esters, M. J. Mehl, A. C. Zettel, Y. Lederer, E. Zurek, J.-P. Maria, D. W. Brenner, X. Campilongo, S. Filipović, W. G. Fahrenholtz, C. J. Ryan, C. M. DeSalle, R. J. Crealese, D. E. Wolfe, A. Calzolari and S. Curtarolo, *Nature*, 2024, **625**, 66–73.
33 K. Kaufmann, D. Maryanovsky, W. M. Mellor, C. Zhu, A. S. Rosengarten, T. J. Harrington, C. Oses, C. Toher, S. Curtarolo and K. S. Vecchio, *npj Comput. Mater.*, 2020, **6**, 42.
34 J. Zhang, B. Xu, Y. Xiong, S. Ma, Z. Wang, Z. Wu and S. Zhao, *npj Comput. Mater.*, 2022, **8**, 1–12.
35 E. Chicardi, C. García-Garrido, J. Hernández-Saz and F. J. Gotor, *Ceram. Int.*, 2020, **46**, 21421–21430.
36 D. Liu, A. Zhang, J. Jia, J. Meng and B. Su, *J. Eur. Ceram. Soc.*, 2020, **40**, 2746–2751.
37 X. F. Wei, Y. Qin, J. X. Liu, F. Li, Y. C. Liang and G. J. Zhang, *J. Eur. Ceram. Soc.*, 2020, **40**, 935–941.
38 S. Kavak, K. G. Bayrak, M. Bellek, S. Mertdinç, F. Muhaffel, H. Gökçe, E. Ayas, B. Derin, M. L. Öveçoğlu and D. Ağaoğulları, *Ceram. Int.*, 2022, **48**, 7695–7705.
39 H. Yang, S. Klemm, J. Müller, M. F. Bekheet, A. Gurlo and D. A. H. Hanaor, *J. Eur. Ceram. Soc.*, 2023, **43**, 4233–4243.
40 T. J. Harrington, J. Gild, P. Sarker, C. Toher, C. M. Rost, O. F. Dippo, C. McElfresh, K. Kaufmann, E. Marin, L. Borowski, P. E. Hopkins, J. Luo, S. Curtarolo, D. W. Brenner and K. S. Vecchio, *Acta Mater.*, 2019, **166**, 271–280.
41 H. R. Mao, E. T. Dong, S. B. Jin, X. M. Qiu and P. Shen, *J. Eur. Ceram. Soc.*, 2022, **42**, 4053–4065.
42 M. Qin, S. Shivakumar, T. Lei, J. Gild, E. C. Hessong, H. Wang, K. S. Vecchio, T. J. Rupert and J. Luo, *J. Eur. Ceram. Soc.*, 2022, **42**, 5164–5171.
43 M. Li, X. Zhao, G. Shao, H. Wang, J. Zhu, W. Liu, B. Fan, H. Xu, H. Lu, Y. Zhou and R. Zhang, *Ceram. Int.*, 2021, **47**, 8707–8710.
44 D. Liu, H. Liu, S. Ning and Y. Chu, *J. Adv. Ceram.*, 2020, **9**, 339–348.
45 Z. Zhang, S. Zhu, F. Z. Dai, H. Xiang, Y. Liu, L. Liu, Z. Ma, S. Wu, F. Liu, K. Sun and Y. Zhou, *J. Mater. Sci. Technol.*, 2022, **121**, 154–162.
46 W. Cao, S. L. Chen, F. Zhang, K. Wu, Y. Yang, Y. A. Chang, R. Schmid-Fetzer and W. A. Oates, *CALPHAD*, 2009, **33**, 328–342.
47 F. Zhang, C. Zhang, S. L. Chen, J. Zhu, W. S. Cao and U. R. Kattner, *CALPHAD*, 2014, **45**, 1–10.
48 C. Zhang and M. C. Gao, *High-Entropy Alloys*, 2016, 399–444.
49 S. Gorsse and O. Senkov, *Entropy*, 2018, **20**, 899.
50 S. Guo, C. Ng, J. Lu and C. T. Liu, *J. Appl. Phys.*, 2011, **109**, 103505.
51 R. Mitra, A. Bajpai and K. Biswas, *Ceram. Int.*, 2022, **48**, 16695–16706.
52 A. Jain, S. P. Ong, G. Hautier, W. Chen, W. D. Richards, S. Dacek, S. Cholia, D. Gunter, D. Skinner, G. Ceder and K. A. Persson, *APL Mater.*, 2013, **1**, 11002.
53 S. P. Ong, W. D. Richards, A. Jain, G. Hautier, M. Kocher, S. Cholia, D. Gunter, V. L. Chevrier, K. A. Persson and G. Ceder, *Comput. Mater. Sci.*, 2013, **68**, 314–319.
54 G. Tallarita, R. Licheri, S. Garroni, R. Orrù and G. Cao, *Scr. Mater.*, 2019, **158**, 100–104.
55 G. Kresse and D. Joubert, *Phys. Rev. B: Condens. Matter Mater. Phys.*, 1999, **59**, 1758.
56 J. P. Perdew, K. Burke and M. Ernzerhof, *Phys. Rev. Lett.*, 1996, **77**, 3865.
57 A. Zunger, S. H. Wei, L. G. Ferreira and J. E. Bernard, *Phys. Rev. Lett.*, 1990, **65**, 353.
58 A. Van de Walle, M. Asta and G. Ceder, *CALPHAD*, 2002, **26**, 539–553.
59 A. Jain, S. P. Ong, G. Hautier, W. Chen, W. D. Richards, S. Dacek, S. Cholia, D. Gunter, D. Skinner, G. Ceder and K. A. Persson, *APL Mater.*, 2013, **1**, 011002.
60 T. H. Fischer and J. Almlóf, *J. Phys. Chem.*, 1992, **96**, 9768–9774.
61 F. Zhang. S. L. Chen and W. S. Cao, PandatTM software, CompuTherm LLC, Madison WI, USA, **https://computherm.com/**, (accessed 3 October 2023).

© 2025 The Author(s). Published by the Royal Society of Chemistry

Open Access Article. Published on 20 May 2025. Downloaded on 1/17/2026 11:19:57 PM.
This article is licensed under a Creative Commons Attribution 3.0 Unported Licence.

62 A. C. Feltrin, D. Hedman and F. Akhtar, *Appl. Phys. Lett.*, 2021, **119**, 161905.
63 L. Ran, S. Guan, W. Liang, J. Pu, P. He, H. Long, P. Yang and F. Peng, *J. Am. Ceram. Soc.*, 2025, **108**, 20368–20374.
64 G. Wang, J. Xu, Y. Chen, Y. J. Zhao, Z. H. Xie and P. R. Munroe, *J. Alloys Compd.*, 2023, **965**, 171342.
65 H. Meng, R. Yu, Z. Tang, Z. Wen, H. Yu and Y. Chu, *Acta Mater.*, 2023, **256**, 119132.
66 B. Bakhit, S. Dorri, A. Kooijman, Z. Wu, J. Lu, J. Rosen, J. M. C. Mol, L. Hultman, I. Petrov, J. E. Greene and G. Greczynski, *Vacuum*, 2021, **185**, 109990.
67 W. G. Fahrenholtz and G. E. Hilmas, *Scr. Mater.*, 2017, **129**, 94–99.
68 S. Wei, M. W. Qureshi, J. Xi, J. Y. Kim, X. Wang, J. Wei, R. Su, L. Liu, W. O. Nachlas, J. H. Perepezko, H. Zhang and I. Szlufarska, *Acta Mater.*, 2024, **267**, 119739.
69 J. Y. Kim, H. Zhang, J. Xi and I. Szlufarska, *Chem. Mater.*, 2022, **34**, 7807–7816.
70 H. Zhang, J. Y. Kim, R. Su, P. Richardson, J. Xi, E. Kisi, J. O'Connor, L. Shi and I. Szlufarska, *Acta Mater.*, 2020, **196**, 505–515.
71 J. Y. Kim, H. Zhang, R. Su, J. Xi, S. Wei, P. Richardson, L. Liu, E. Kisi, J. H. Perepezko and I. Szlufarska, *Acta Mater.*, 2022, **235**, 118099.
72 M. Qin, J. Gild, H. Wang, T. Harrington, K. S. Vecchio and J. Luo, *J. Eur. Ceram. Soc.*, 2020, **40**, 4348–4353.
73 C. Wang, M. Qin, T. Lei, Y. He, K. Kisslinger, T. J. Rupert, J. Luo and H. L. Xin, *J. Eur. Ceram. Soc.*, 2021, **41**, 5380–5387.
74 F. Zhang and U. Kattner, *J. Phase Equilib. Diffus.*, 2015, **36**, 1–2.
75 T. Abe, *Mater. Trans.*, 2021, **62**, 711–718.
76 S. Wei, M. W. Qureshi, J. Wei, X. Hu, L. Liu, J. Xi, S. Attarian, R. Su, H. Zhang, E. Willing, X. Wang, K. Sridharan, P. M. Voyles, John H. Perepezko and I. Szlufarska, Short-range order in high entropy carbide, Submitted.
77 C.-Y. He, Y. Li, Z.-H. Zhou, B.-H. Liu, X.-H. Gao, C.-Y. He, Z.-H. Zhou, B.-H. Liu, X.-H. Gao and Y. Li, *Adv. Mater.*, 2024, **36**, 2400920.
78 T. J. Boerner, S. Deems, T. R. Furlani, S. L. Knuth and J. Towns, PEARC 2023 – Computing for the common good: Practice and Experience in Advanced Research Computing, 2023, pp. 173–176.


© 2025 The Author(s). Published by the Royal Society of Chemistry